

# Tensile-strained germanium microdisk electroluminescence

M. Prost,<sup>1,2</sup> M. El Kurdi,<sup>1</sup> A. Ghrib,<sup>1</sup> S. Sauvage,<sup>1</sup> X. Checoury,<sup>1</sup> N. Zerounian,<sup>1</sup> F. Aniel,<sup>1</sup> G. Beaudoin,<sup>3</sup> I. Sagnes,<sup>3</sup> F. Boeuf,<sup>2</sup> and P. Boucaud<sup>1,\*</sup>

<sup>1</sup>*Institut d'Electronique Fondamentale, CNRS - Univ. Paris Sud 11, Bâtiment 220, F-91405 Orsay, France*

<sup>2</sup>*STMicroelectronics, 850 Rue Jean Monnet, F-38920 Crolles, France*

<sup>3</sup>*Laboratoire de Photonique et de Nanostructures, CNRS - UPR 20, Route de nozay, F-91460 Marcoussis, France*

\*[philippe.boucaud@ief.u-psud.fr](mailto:philippe.boucaud@ief.u-psud.fr)

<http://pages.ief.u-psud.fr/QDgroup>

**Abstract:** We report room temperature electroluminescence of tensile-strained germanium microdisks. The strain is transferred into the microdisks using silicon nitride stressors. Carrier injection is achieved with Schottky contacts on *n*-type doped germanium. We show that a biaxial tensile-strain up to 0.72% can be transferred by optimizing the carrier injection profile. The transferred strain is measured by the electroluminescence spectral red-shift and compared to finite element modeling. We discuss the impact of this strain level to achieve population inversion in germanium.

© 2015 Optical Society of America

**OCIS codes:** (230.3670) Light-emitting diodes ; (300.6470) Spectroscopy, semiconductors.

---

## References

1. R. E. Camacho-Aguilera, Y. Cai, N. Patel, J. T. Bessette, M. Romagnoli, L. C. Kimerling, and J. Michel, "An electrically pumped germanium laser," *Opt. Express* **20**, 11316–11320 (2012).
2. B. Dutt, D. S. Sukhdeo, D. Nam, B. M. Vulovic, Z. Yuan, and K. C. Saraswat, "Roadmap to an efficient germanium-on-silicon laser: Strain vs. n-type doping," *IEEE Photonics J.* **4**, 2002–2009 (2012).
3. Y. Ishikawa, K. Wada, D. D. Cannon, J. Liu, H.-C. Luan, and L. C. Kimerling, "Strain-induced band gap shrinkage in Ge grown on Si substrate," *Appl. Phys. Lett.* **82**, 2044 (2003).
4. M. J. Suess, R. Geiger, R. A. Minamisawa, G. Schiefler, J. Frigerio, D. Chrastina, G. Isella, R. Spolenak, J. Faist, and H. Sigg, "Analysis of enhanced light emission from highly strained germanium microbridges," *Nature Photon* **7**, 466–472 (2013).
5. D. S. Sukhdeo, D. Nam, J.-H. Kang, M. L. Brongersma, and K. C. Saraswat, "Direct bandgap germanium-on-silicon inferred from 5.7% tensile strain," *Photon. Res.* **2**, A8–A13 (2014).
6. J. R. Sanchez-Prez, C. Boztug, F. Chen, F. F. Sudradjat, D. M. Paskiewicz, R. Jacobson, M. G. Lagally, and R. Paiella, "Direct-bandgap light-emitting germanium in tensilely strained nanomembranes," *Proc. Nat. Acad. Sci.* **108**, 18893–18898 (2011).
7. A. Ghrib, M. de Kersauson, M. El Kurdi, R. Jakomin, G. Beaudoin, S. Sauvage, G. Fishman, G. Ndong, M. Chaigneau, and R. Ossikovski, "Control of tensile strain in germanium waveguides through silicon nitride layers," *Appl. Phys. Lett.* **100**, 201104 (2012).
8. J. R. Jain, A. Hryciw, T. M. Baer, D. A. B. Miller, M. L. Brongersma, and R. T. Howe, "A micromachining-based technology for enhancing germanium light emission via tensile strain," *Nature Photon* **6**, 398–405 (2012).
9. G. Capellini, G. Kozłowski, Y. Yamamoto, M. Lisker, C. Wenger, G. Niu, P. Zaumseil, B. Tillack, A. Ghrib, and M. de Kersauson, "Strain analysis in SiN/Ge microstructures obtained via Si-complementary metal oxide semiconductor compatible approach," *J. Appl. Phys.* **113**, 013513 (2013).
10. S.-L. Cheng, J. Lu, G. Shambat, H.-Y. Yu, K. Saraswat, J. Vuckovic, and Y. Nishi, "Room temperature 1.6  $\mu\text{m}$  electroluminescence from Ge light emitting diode on Si substrate," *Opt. Express* **17**, 10019–10024 (2009).

11. S.-L. Cheng, G. Shambat, J. Lu, H.-Y. Yu, K. Saraswat, T. I. Kamins, J. Vuckovic, and Y. Nishi, "Cavity-enhanced direct band electroluminescence near 1550 nm from germanium microdisk resonator diode on silicon," *Appl. Phys. Lett.* **98**, 211101 (2011).
12. D. Nam, D. Sukhdeo, S.-L. Cheng, A. Roy, K. Chih-Yao Huang, M. Brongersma, Y. Nishi, and K. Saraswat, "Electroluminescence from strained germanium membranes and implications for an efficient Si-compatible laser," *Appl. Phys. Lett.* **100**, 131112 (2012).
13. M. Kaschel, M. Schmid, M. Gollhofer, J. Werner, M. Oehme, and J. Schulze, "Room-temperature electroluminescence from tensile strained double-heterojunction germanium pin LEDs on silicon substrates," *Solid-State Electron.* **83**, 87–91 (2013).
14. M. Schmid, M. Oehme, M. Gollhofer, R. Krner, M. Kaschel, E. Kasper, and J. Schulze, "Effect of heavy doping and strain on the electroluminescence of Ge-on-Si light emitting diodes," *Thin Sol. Films* **557**, 351–354 (2014).
15. M. de Kersauson, M. El Kurdi, S. David, X. Checoury, G. Fishman, S. Sauvage, R. Jakomin, G. Beaudoin, I. Sagnes, and P. Boucaud, "Optical gain in single tensile-strained germanium photonic wire," *Opt. Express* **19**, 17925–17934 (2011).
16. R. Jakomin, M. de Kersauson, M. El Kurdi, L. Largeau, O. Mauguin, G. Beaudoin, S. Sauvage, R. Ossikovski, G. Ndong, and M. Chaigneau, "High quality tensile-strained n-doped germanium thin films grown on InGaAs buffer layers by metal-organic chemical vapor deposition," *Appl. Phys. Lett.* **98**, 091901 (2011).
17. M. de Kersauson, M. Prost, A. Ghrib, M. El Kurdi, S. Sauvage, G. Beaudoin, L. Largeau, O. Mauguin, R. Jakomin, and I. Sagnes, "Effect of increasing thickness on tensile-strained germanium grown on InGaAs buffer layers," *J. Appl. Phys.* **113**, 183508 (2013).
18. M. Prost, M. El Kurdi, A. Ghrib, X. Checoury, N. Zerounian, F. Aniel, G. Beaudoin, I. Sagnes, C. Baudot, and F. Boeuf, "Schottky electroluminescent diodes with n-doped germanium," *Appl. Phys. Lett.* **104**, 241104 (2014).
19. M. El Kurdi, T. Kociniowski, T.-P. Ngo, J. Boulmer, D. Debarre, P. Boucaud, J. F. Damlencourt, O. Kermerrec, and D. Bensahel, "Enhanced photoluminescence of heavily n-doped germanium," *Appl. Phys. Lett.* **94**, 191107 (2009).
20. J. S. Xia, K. Nemoto, Y. Ikegami, Y. Shiraki, and N. Usami, "Silicon-based light emitters fabricated by embedding Ge self-assembled quantum dots in microdisks," *Appl. Phys. Lett.* **91**, 011104 (2007).
21. A. Ghrib, M. El Kurdi, M. de Kersauson, M. Prost, S. Sauvage, X. Checoury, G. Beaudoin, I. Sagnes, and P. Boucaud, "Tensile-strained germanium microdisks," *Appl. Phys. Lett.* **102**, 221112 (2013).
22. M. El Kurdi, H. Bertin, E. Martincic, M. de Kersauson, G. Fishman, S. Sauvage, A. Bosseboeuf, and P. Boucaud, "Control of direct band gap emission of bulk germanium by mechanical tensile strain," *Appl. Phys. Lett.* **96**, 041909 (2010).
23. P. Boucaud, M. El Kurdi, A. Ghrib, M. Prost, M. de Kersauson, S. Sauvage, F. Aniel, X. Checoury, G. Beaudoin, and L. Largeau, "Recent advances in germanium emission," *Phot. Res.* **1**, 102 (2013).
24. M. El Kurdi, G. Fishman, S. Sauvage, and P. Boucaud, "Band structure and optical gain of tensile-strained germanium based on a 30 band k.p formalism," *J. Appl. Phys.* **107**, 013710 (2010).
25. D. Nam, D. S. Sukhdeo, J.-H. Kang, J. Petykiewicz, J. H. Lee, W. S. Jung, J. Vuckovic, M. L. Brongersma, and K. C. Saraswat, "Strain-induced pseudoheterostructure nanowires confining carriers at room temperature with nanoscale-tunable band profiles," *Nano Letters* **13**, 3118–3123 (2013).
26. G. Shambat, S.-L. Cheng, J. Lu, Y. Nishi, and J. Vuckovic, "Direct band Ge photoluminescence near 1.6  $\mu\text{m}$  coupled to Ge-on-Si microdisk resonators," *Appl. Phys. Lett.* **97**, 241102 (2010).

---

## 1. Introduction

An electrically-pumped germanium laser on silicon has been recently reported using a moderate biaxial tensile strain (0.25%) and heavy *n*-type doping [1]. It has been theoretically shown that the current threshold to achieve lasing could be significantly reduced by increasing the amount of tensile strain in germanium [2]. There are several approaches to apply a tensile strain on a germanium layer. The standard one relies on the thermal expansion mismatch during the growth process of germanium on silicon at high temperature [3]. It can lead to a biaxial tensile strain of approximately 0.25% in the germanium layer. This initial strain can be amplified using geometrical patterning of the layers in form of microbridges [4,5]. Very high strain amplitudes can also be obtained on mechanically-strained nanomembranes [6] but these structures are not adapted for lasing. Another approach relies on strain transfer by an external stressor like SiN [7–9]. This approach is very attractive since one has to keep in mind that a germanium laser represents a significant interest for silicon photonics only if it can be operated at room temperature under electrical injection [10–14]. The transfer of tensile strain has thus to be compatible with electrical injection.

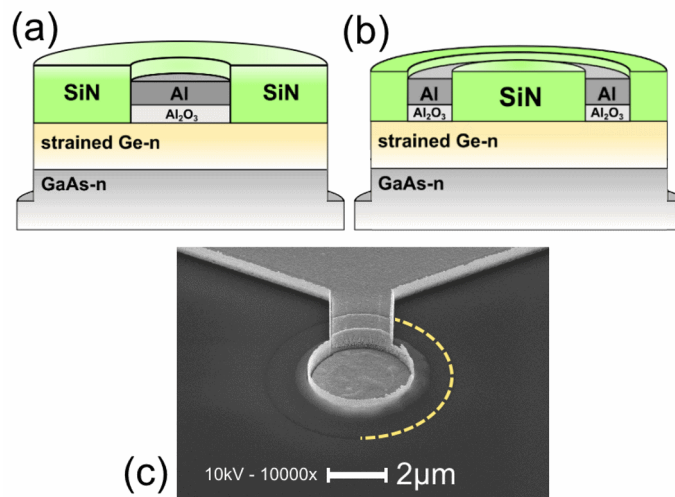


Fig. 1. Schematic cross-section of the germanium microdisk diode with (a) disk-shaped and (b) annular contact. (c) Scanning electron microscope image of the fabricated microdisk with electrical injection for the disk-shaped contact configuration. The microdisk is buried under the SiN layer, a line is drawn to indicate the position of the microdisk edge.

In this work, we report on room temperature electroluminescence with tensile-strained germanium. We use silicon nitride stressors (SiN) to apply a tensile strain, a method that is compatible with complementary metal oxide semiconductor (CMOS) processing environment. We investigate different designs for electrical injection either using disk-shaped or annular Schottky contacts on *n*-doped germanium microdisks. The transferred tensile strain is estimated by the room temperature electroluminescence spectral shift of direct band gap recombination. We show that an average biaxial tensile strain up to 0.72% can be obtained with annular contacts. We finally discuss the impact of these results to achieve population inversion in germanium.

## 2. Sample fabrication

The studied samples were fabricated in a metal-organic vapor phase epitaxy reactor that can handle both germanium and III–V elements [15–17]. Isobutylgermane is used as precursor for the germanium. The *n*-doped Ge layers are directly grown on an *n*-doped GaAs substrate with a doping level of  $10^{18} \text{ cm}^{-3}$ . This provides a high quality Ge layer without an interfacial defective region, as Ge and GaAs are nearly lattice-matched. The Ge thickness is 250 nm and its *n*-doping is around  $1\text{--}1.5 \times 10^{19} \text{ cm}^{-3}$ . The *n*-type GaAs substrate has a higher band gap thus forming an heterostructure at the Ge/GaAs interface. This heterostructure allows electron injection and carrier confinement in the germanium layer. Figs. 1(a) and 1(b) present the schematic cross-section of the germanium microdisk diode with disk-shaped and with annular contacts respectively. For a  $9 \mu\text{m}$  diameter microdisk, the disk-shaped metal contact has a  $6 \mu\text{m}$  diameter. The annular contact is 500 nm thin with an inner diameter of  $3 \mu\text{m}$ . A plan view image by scanning electron microscope of a fully processed device is shown in Fig. 1(c). As the device is buried under a SiN layer, we only see the edge of the microdisk. The ohmic backside contact on the GaAs substrate is formed by an Au/Ge/Ni/Au metal deposition followed by a rapid thermal annealing. E-beam lithography and an inductively-coupled plasma (ICP) etching of germanium were applied to define microdisks with various diameter sizes. This step is followed by  $1.8 \mu\text{m}$  vertical etching of the GaAs substrate. It leads to a pillar configuration that ensures the spreading of

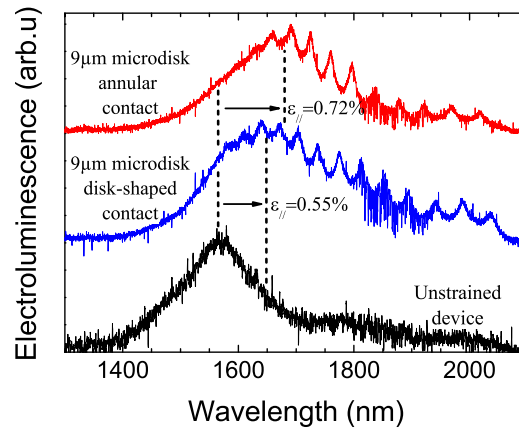


Fig. 2. Normalized room temperature electroluminescence spectra of an unstrained germanium device (black curve-bottom), 9  $\mu\text{m}$  diameter microdisk with disk-shaped contact (blue curve-middle) and 9  $\mu\text{m}$  diameter microdisk with annular contact (red curve-top). The spectra are normalized and offset for clarity.

injected carriers in the whole germanium layer under electrical pumping without the problems of electrical injection in underetched microdisks with small posts. The structure is then coated by a 350 nm thick layer of silicon nitride using plasma-enhanced chemical vapor deposition (PECVD) [7]. The compressively-strained SiN layer allows passivation and electrical insulation of the germanium. Its most important feature is to transfer tensile strain in germanium during its mechanical relaxation. After opening contact windows in the SiN layer by ICP dry etching with  $\text{C}_4\text{F}_8$  and  $\text{SF}_6$  gases, the top contact is deposited by e-beam evaporation. Prior to Al deposition, a thin layer of  $\text{Al}_2\text{O}_3$  (1.5 nm) is deposited using an electron beam evaporator to passivate the interfacial states between germanium and the metal, resulting in an enhancement of carrier injection and improvement of electroluminescence efficiency [18]. Strained structures with two different contact geometries as shown in Fig. 1 were processed. We have used, as reference unstrained samples, devices fabricated in the same run without lateral microdisk patterning. In the latter case, the strain transfer vanishes. We have checked that the peak recombination for these samples was similar to the one measured on standard unstrained electroluminescence germanium diodes. Using such reference sample avoids the need of a second processing run with its five lithography steps.

### 3. Electroluminescence

The room temperature (295 K) electroluminescence was collected from the top surface with a near-infrared x20 objective (numerical aperture 0.35) coupled to an extended InGaAs multi-channel detector. Experiments were performed in a standard laboratory environment. Figure 2 shows the spectra obtained with an unstrained germanium device and for 9  $\mu\text{m}$  diameter microdisks with disk-shaped and annular Schottky contacts. The unstrained device is not a microdisk. The spectra amplitudes are normalized to unity for comparison. The electroluminescence intensities were not compared because the device designs are different between the unstrained one and the strained microdisks. These measurements are performed under minimal current injection to achieve electroluminescence observation ( $\sim 1\text{mA}$ ), in order to avoid any thermal heating of the device. For the unstrained device, the emitted light is dominated by the

direct band gap recombination [19], the peak maximum of emission is located around 1560 nm. The indirect band gap recombination can be observed at longer wavelength as a shoulder around 1800 nm. The spectrum in the middle of Fig. 2 is obtained for a 9  $\mu\text{m}$  diameter microdisk with a disk-shaped contact. The direct band gap and indirect band gap recombinations are modulated by a series of broad resonances, associated with Fabry-Perot modes along the disk diameter [20,21]. We have not observed any whispering gallery modes since the geometry is not favorable to collect the scattered light emission from these modes. In the central part of the microdisk, the light emission is masked by the metallic contact. The light is collected from the edge of the structure, where the SiN layer applies the strain. A spectral shift of the near-infrared emitted light is clearly observed, and we estimate the peak maximum position for direct band gap recombination around 1650 nm. The position of the peak maximum on strain-free device germanium is used as a reference to compare the total red-shift. The total red-shift is thus 90 nm which corresponds to an energy reduction of 43 meV. This value corresponds to an equivalent transferred biaxial strain of  $\epsilon_{\parallel} = 0.55\% \pm 0.015\%$  if we consider the recombination between the zone center  $\Gamma$  valley and the heavy hole band [22]. We have checked by simulation that for the investigated strain transfers, the electroluminescence is indeed dominated by the recombination with the heavy hole band for carrier injection larger than  $10^{17} \text{ cm}^{-3}$ , in agreement with the applied current densities. We observe that the electroluminescence spectra of the strained microdisks are broadened as compared to the unstrained ones. This effect is a consequence of the strain gradient and of the light and heavy hole splitting. As shown on the top spectrum of Fig. 2, the maximum of direct band gap recombination for the device with the annular contact is around 1680 nm. The position of maximum is thus red-shifted by an additional 30 nm as compared to the previous diode. The reduction of energy separation is about 56 meV, and the estimated equivalent biaxial strain is up to  $0.72\% \pm 0.021\%$  on this device. The strain transfer is thus significantly improved by reducing the metallic contact size. Consequently, the SiN layer covers a larger surface and the blocking of strain transfer by the metal is reduced. We can also observe that the positions of the peaks associated with Fabry-Perot modes along the disk diameter are shifted by a half-period. This effect can be explained by the slight modification of the effective refractive index of the guided mode by the metallic contact. We note that these devices have reached a level of strain equal to the one reported for a germanium diode in [12], but the latter device with a backside tungsten stressor was not adapted for integration. In our case, the structure is an optical resonator combined with an active zone in  $n$ -doped and strained germanium. The tensile strain is larger by a factor of 3 as compared to standard Ge on Si diodes. We emphasize that the strain transfer would be even more reinforced for a germanium layer grown on silicon as we could benefit from strain due to thermal dilatation coefficients mismatch.

#### 4. Strain field analysis

We have performed finite element modeling of the strain field in the germanium in order to estimate the theoretical achievable strain in different devices. The material parameters used are similar to those from previous works. A 1.8 GPa in-plane stress was measured in the nitride film after deposition in similar conditions on a silicon substrate. The initial stress in the nitride is described by an equivalent hydrostatic strain in the modeling [7,23]. Figs. 3(a) and 3(b) show the trace of the strain field components ( $\epsilon_r + \epsilon_{\theta} + \epsilon_z$ ) obtained by finite element modeling in the full device with disk-shaped and annular contact in case of axi-symmetric simulations. We represent the trace, i.e. the hydrostatic strain, as the energy difference between L and  $\Gamma$  valleys depends directly on this parameter [24]. The transferred strain is maximum at the interface between the SiN and the germanium layers. Its amplitude decreases progressively along the depth of the germanium layer. The trace of the strain field increases towards the edge of the microdisk. It is a consequence of the presence of silicon nitride at the microdisk edge. We show

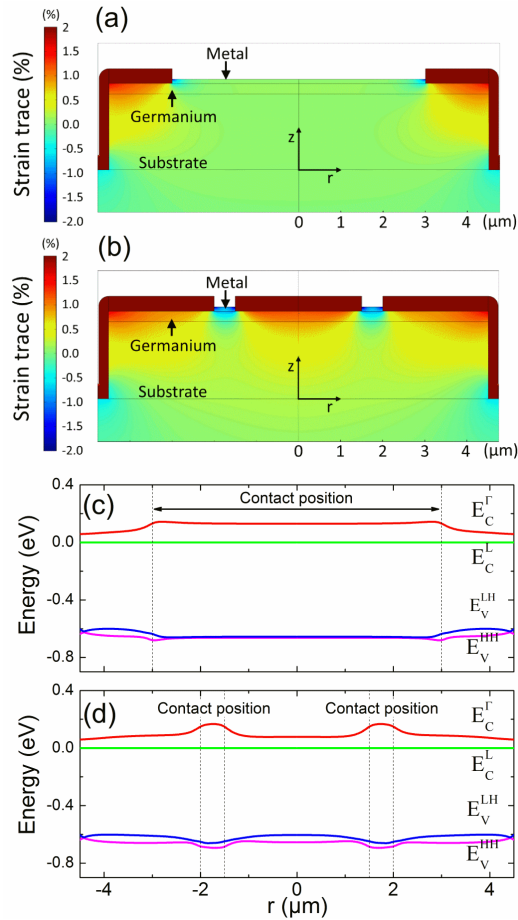


Fig. 3. Finite element modeling of the strain profile for a  $9 \mu\text{m}$  diameter microdisk device for the configuration with (a) disk-shaped contact and (b) annular contact. The trace of the strain field ( $\epsilon_r + \epsilon_{theta} + \epsilon_z$ ) is represented. Calculated band diagram along the lateral direction of the germanium at the middle-height of the layer for the disk-shaped (c) and for the annular contact configuration (d).

in figure 3(c) and 3(d), a two-dimensional energy band diagram along the lateral direction at the middle height of the germanium layer for the disk-shaped and annular contacts respectively, as obtained with a 30 band  $\mathbf{k}\cdot\mathbf{p}$  formalism. The figures represent the spatially-resolved energy position of the  $\Gamma$ , and L conduction bands and of the heavy hole and light hole bands. We can visualize the impact of the contact position to the local bandgap energy modification leading to a pseudo-heterostructure configuration similar to the one observed in germanium microbridge under optical pumping [25]. The strain gradient pushes the carriers to regions with an energy minimum away from the metal contacts. As seen in Fig. 3(a), beneath the metallic contact, the averaged strain amplitude is close to zero. Whereas outside of the metal the volume-averaged tensile strain amplitude is about 0.53% in biaxial approximation. A good agreement is found with the experimental measurement where an equivalent value of 0.55% biaxial strain is measured. Fig. 3(b) shows the annular contact configuration. A tight zone is under compression beneath the metallic contact. Experimentally, we have observed that the light is mainly emitted from the center of the structure. We only consider the  $2\ \mu\text{m}$  center zone of the microdisk to calculate the volume-averaged tensile strain amplitude. It is around 0.63% in biaxial approximation as compared to the measured value of 0.72%. The small variation with the experimental value can result from the difficulty to estimate properly the area where light emission occurs. The electroluminescence is dependent on the minority carrier injection and the spatial distribution of carriers in germanium. As we can observe electroluminescence from the strained part of the device, the lateral hole current in the structure is crucial. The hole current is not only dominated by a vertical current under the contact. An application of a positive bias lowers the energy band positions below the contact, leading to the formation of a potential barrier for the holes. This induces a lateral hole diffusion outwards the contact region. This effect is strengthened by the reduction of the bandgap energy due to the tensile strain, as can be seen in Figs. 3(c) and 3(d). The lateral hole injection can thus be optimized through the metal size reduction and by increasing the tensile strain and the energy band gradient below the contact due to the applied potential.

## 5. Current density dependence

Figures 4(a) and 4(b) present the spectra under various values of continuous current injection, for the microdisk with disk-shaped and annular contacts respectively. The diodes are operated at forward current in the mA range. A mA corresponds to a current density of  $1.5\ \text{kA cm}^{-2}$  for a  $9\ \mu\text{m}$  diameter disk. The quality factors of the different resonances are found around 100, which is close to those measured with similar structures under optical pumping [21]. We can conclude that the losses introduced by the metallic contact remains low as compared to the losses at the germanium/nitride/air interface. The quality factors remain constant as the cw pump current is increased up to 12.5 mA. The range of applied current density does not allow to reach the condition where the gain can compensate the absorption losses. We observe that there is no spectral shift as the current density is increased, thus confirming that the electroluminescence is dominated by the heavy hole recombination, even at small injection. We have investigated several sizes of microdisk from 6 to  $12\ \mu\text{m}$  for the devices with a disk-shaped contact. Figure 4(c) presents the integrated electroluminescence signal versus the current density in the device. The integrated signal is linear after a threshold in current. It occurs at a value around  $5\ \text{kA cm}^{-2}$ . This threshold effect could be associated with the onset of an effective lateral hole injection when the energy bands are lowered by the applied bias. Consequently, the electroluminescence signal becomes significant. The breakdown of the device occurs for injected current larger than 5-15 mA depending on the microdisk size. This limit can be avoided by using pulsed current injection, allowing to increase the current by a factor 5. The pulse duration was 500 ns and the duty cycle 10 %. The current value was monitored by a current transformer probe.

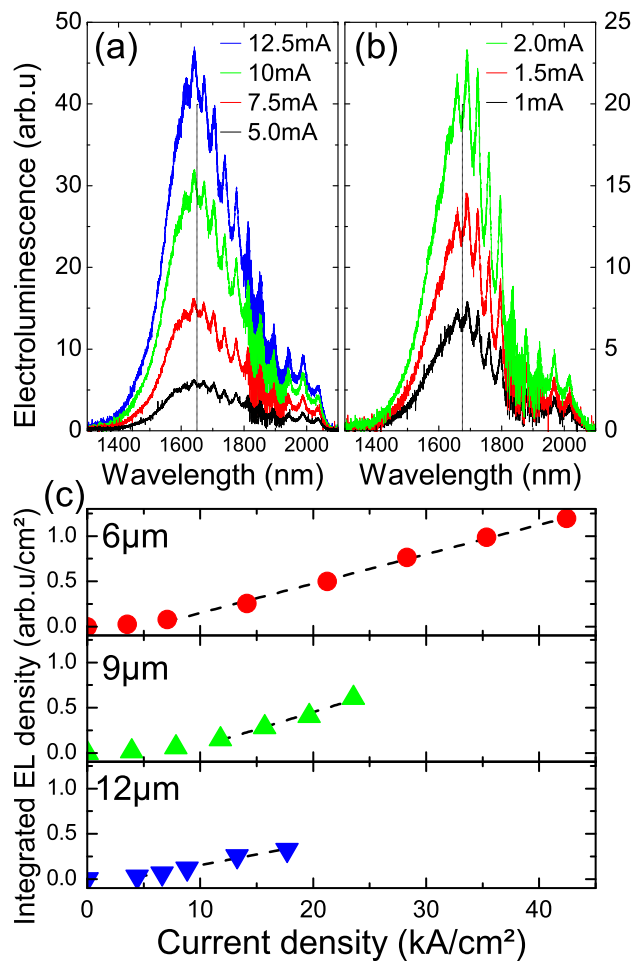


Fig. 4. Room temperature electroluminescence spectra under different injection current for the disk-shaped contact (a) and annular contact (b) configuration for 9  $\mu\text{m}$  diameter microdisk. The metal contact has a 6  $\mu\text{m}$  diameter in (a). The annular contact in (b) is 500 nm thin with an inner diameter of 3  $\mu\text{m}$ . (c) Integrated electroluminescence optical density for 6, 9, and 12  $\mu\text{m}$  diameter microdisks with disk-shaped contact configuration as a function of current density. The dashed lines are linear guides to the eye.

As we increase the pulsed pump current, the Fabry-Perot resonant peaks are broadened due to free carrier absorption [26]. We note that as long as the devices are operated under the above-mentioned current conditions either in cw or pulsed experiments, the device reliability is excellent. For larger current values, failure of the devices occurs because of a degradation of the metal contacts.

We have performed electrical simulations in order to evaluate the current density threshold to obtain population inversion in a germanium double heterostructure. For a germanium layer doped at  $1 \times 10^{19} \text{ cm}^{-3}$  with a 0.7% biaxial strain, the current density threshold is estimated around  $200 \text{ kA cm}^{-2}$ . This value is not reasonable for device reliability. With this level of strain, the current density could be reduced below the  $10 \text{ kA cm}^{-2}$  range by increasing the doping level up to  $5 \times 10^{19} \text{ cm}^{-3}$ . If the biaxial strain in the microdisk is increased up to 1%

by using for example a germanium layer grown on silicon, the necessary doping level is thus reduced at  $4 \times 10^{19} \text{cm}^{-3}$  to obtain the population inversion in germanium below the  $10 \text{ kA cm}^{-2}$  range.

## 6. Conclusion

In conclusion, we have shown room-temperature electroluminescence with *n*-doped and tensile-strained germanium layers. We use Schottky contacts to perform carrier injection in a resonant device with a tensile biaxial strain up to 0.72%. The impact of the metal is minimized using a low area contact configuration, either in the case of strain transfer, or for the optical properties, as the obtained results by electroluminescence are similar to the one under optical pumping. Thus by optimizing the process, and starting on germanium on silicon layer, with an initial strain of 0.25%, the total amount of strain is foreseen to be close to 1.0% and the current density threshold to reach population inversion could be drastically reduced below the  $10 \text{ kA cm}^{-2}$  range.

## Acknowledgments

This work was supported by Agence Nationale de la Recherche under GRAAL convention (ANR 2011 B S03 004 01) and by “Triangle de la Physique” under Gerlas convention. This work was also partly supported by the RENATECH network and by Région Ile de France (C’Nano2011-Nanoetch project). M. Prost is funded by a CIFRE Grant.